LETTER

doi:10.1038/nature25020

A brief visit from a red and extremely elongated interstellar asteroid

Karen J. Meech[1], Robert Weryk[1]*, Marco Micheli[2,3]*, Jan T. Kleyna[1]*, Olivier R. Hainaut[4]*, Robert Jedicke[1], Richard J. Wainscoat[1], Kenneth C. Chambers[1], Jacqueline V. Keane[1], Andreea Petric[1], Larry Denneau[1], Eugene Magnier[1], Travis Berger[1], Mark E. Huber[1], Heather Flewelling[1], Chris Waters[1], Eva Schunova-Lilly[1] & Serge Chastel[1]

None of the approximately 750,000 known asteroids and comets in the Solar System is thought to have originated outside it, despite models of the formation of planetary systems suggesting that orbital migration of giant planets ejects a large fraction of the original planetesimals into interstellar space[1]. The high predicted number density[2] of icy interstellar objects (2.4×10^{-4} per cubic astronomical unit) suggests that some should have been detected, yet hitherto none has been seen. Many decades of asteroid and comet characterization have yielded formation models that explain the mass distribution, chemical abundances and planetary configuration of the Solar System today, but there has been no way of telling whether the Solar System is typical of planetary systems. Here we report observations and analysis of the object 1I/2017 U1 ('Oumuamua) that demonstrate its extrasolar trajectory, and that thus enable comparisons to be made between material from another planetary system and from our own. Our observations during the brief visit by the object to the inner Solar System reveal it to be asteroidal, with no hint of cometary activity despite an approach within 0.25 astronomical units of the Sun. Spectroscopic measurements show that the surface of the object is spectrally red, consistent with comets or organic-rich asteroids that reside within the Solar System. Light-curve observations indicate that the object has an extremely oblong shape, with a length about ten times its width, and a mean radius of about 102 metres assuming an albedo of 0.04. No known objects in the Solar System have such extreme dimensions. The presence of 'Oumuamua in the Solar System suggests that previous estimates of the number density of interstellar objects, based on the assumption that all such objects were cometary, were pessimistically low. Planned upgrades to contemporary asteroid survey instruments and improved data processing techniques are likely to result in the detection of more interstellar objects in the coming years.

On 2017 October 19 the Pan-STARRS1 telescope system detected an object moving rapidly west at 6.2° per day (Fig. 1a). A search of images from previous nights found that the object had also been imaged on October 18. Additional images acquired with the Canada–France–Hawaii telescope (CFHT) on October 22 confirm that this object has highest known hyperbolic eccentricity of 1.188 ± 0.016 (ref. 3). Data obtained by us and others during the period October 14–30 refine the orbital eccentricity of the object to 1.1956 ± 0.0006—a level of precision that confirms the hyperbolic nature to more than 100σ. (Unless otherwise stated, the errors quoted are 1σ.) Designated as 1I/2017 U1, this object is clearly from outside the Solar System (Fig. 2) and as such is the first interstellar object (ISO) to have been detected. Given its discovery and follow-up observations from multiple observatories in Hawaii, 1I/2017 U1 has been named 'Oumuamua, which in Hawaiian reflects the way that this object is like a scout or messenger sent from the distant past to reach out to us.

The October 22 CFHT observations were tracked at the rate of motion of the object; its point-spread function was consistent with a stellar profile with no asymmetry and no coma, implying that it is

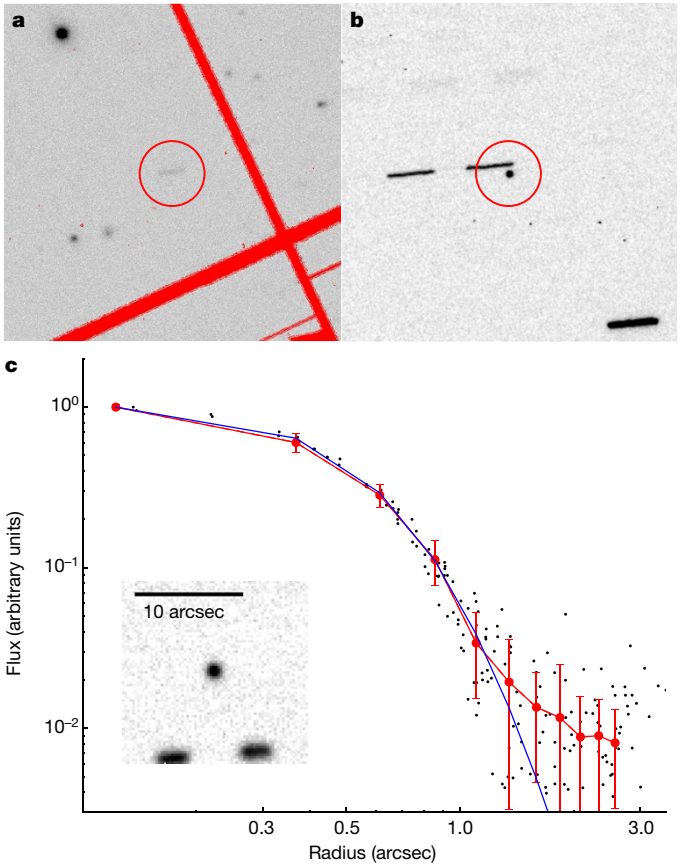

Figure 1 | The asteroidal appearance of 'Oumuamua. a, Pan-STARRS1 discovery image of 'Oumuamua on 2017 October 19: 'Oumuamua is the faint trail centred in the red circle. Red regions are masked pixels. **b**, CFHT image obtained on October 22 guided at the rate of 'Oumuamua, which shows up as a point, whereas the stars are trailed. There is no extended scattered light around 'Oumuamua, that is, no hint of a dust coma. **c**, A deep image combining Gemini and VLT *g*- and *r*-band data is shown in the inset. In the main panel, the black points mark the flux in individual pixels. The red circles show the average flux in annuli at each radius (the error bars are the root-mean-square dispersion) and the blue line is a Moffat profile with a full-width at half-maximum (FWHM) of 0.87″. The difference between the two curves provides a very sensitive upper limit for any possible activity.

[1]Institute for Astronomy, 2680 Woodlawn Drive, Honolulu, Hawaii 96822, USA. [2]ESA SSA-NEO Coordination Centre, Largo Galileo Galilei 1, 00044 Frascati, Italy. [3]Osservatorio Astronomico di Roma, Via Frascati 33, 00040 Monte Porzio Catone, Italy. [4]European Southern Observatory, Karl-Schwarzschild-Strasse 2, D-85748 Garching bei München, Germany.
*These authors contributed equally to this work.

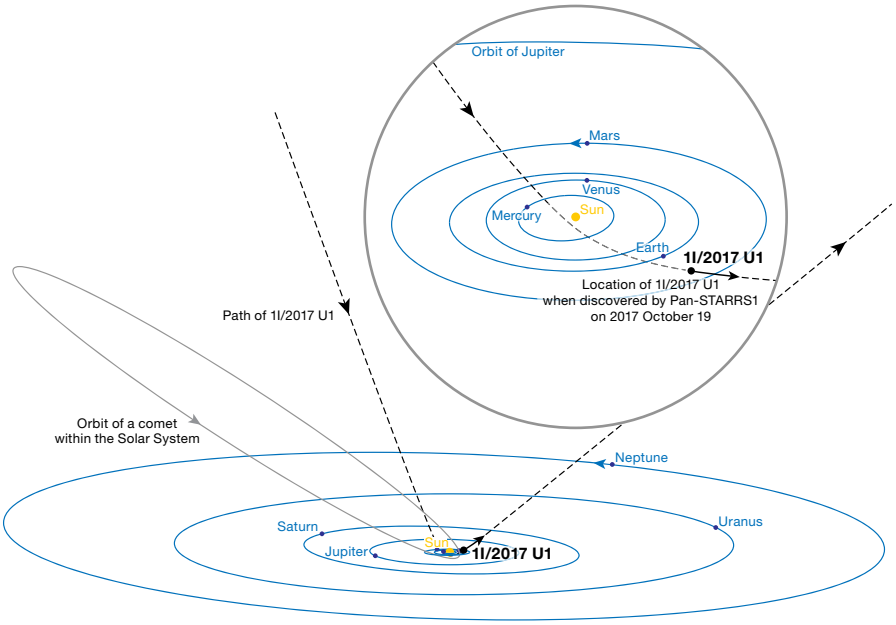

Figure 2 | The path of 'Oumuamua (1I/2017 U1) through the Solar System. The orbit of a typical Halley-type comet is shown for comparison as the solid grey line. The inset shows the inner Solar System; the solid line segment along the trajectory taken by 'Oumuamua (otherwise dashed) indicates the short window of two weeks during which it was bright enough (median light-curve magnitude $V = 20–24$ mag) to be studied by large telescopes on Earth. The path is shown in grey when the object was below the ecliptic. Image adapted from http://www.ifa.hawaii.edu/info/press-releases/interstellar/, Brooks Bays/SOEST Publication Services/University of Hawaii, Institute for Astronomy.

asteroidal (Fig. 1b). Additional time-resolved sequences of images at multiple wavelengths on October 25–27 UT with the European Southern Observatory (ESO) Very Large Telescope (VLT) and the Gemini South Telescope, further strengthened identification of 'Oumuamua as asteroidal (Fig. 1c). The upper limit for the dust coma brightness is $g > 25.8$ mag in the wings of point-spread function (1″–2″ from the centre) of the object and $g > 29.8 \pm 0.05$ mag arcsec^{-2} at the 5σ level outside the point-spread function (more than 5″ from the centre). Using the upper limit for the light that could be scattered by dust, we determined that less than 1.7×10^{-3} kg s^{-1} of dust could have been released from the surface. This is 7–8 orders of magnitude less than a typical long-period comet would produce if there was near-surface water ice (see Methods).

An analysis of the light curve of 'Oumuamua (Fig. 3, see Methods) indicates that its rotation period is 7.34 ± 0.06 h under the customary assumption that the double-peaked light curve is dominated by the shape of the object. No other period gives a satisfactory re-phased light curve and the value is not unusual for objects of this size.

The median magnitude of 'Oumuamua gives it an average radius of about 100 m assuming an albedo of 0.04, but the very large, 2.5 mag light-curve range implies that it is extremely elongated, with an axis ratio of at least 10:1 (see Methods), or that it has large albedo variations, or both. Its red surface colour is consistent with the organic-rich surfaces of comets, D-type asteroids and outer-Solar-System small bodies (Fig. 4). Its measured colours ($g - r = 0.84 \pm 0.05$ mag, $g - i = 1.15 \pm 0.10$ mag, $g - z = 1.25 \pm 0.10$ mag and $g - Y = 1.60 \pm 0.20$ mag), which correspond to a spectral slope of $S_\nu = 23\% \pm 3\%$ per 100 nm), are consistent with uniform colours over the whole surface of the object (see Methods). This uniform colouring suggests that the reflectivity of 'Oumuamua is indistinguishable from that of small bodies in the Solar System; but the inferred shape is unique.

The highly elongated shape of 'Oumuamua that is implied by its large light-curve range is very unusual. If the object is long and cylindrical and rotating around its shortest axis, it must have at least some tensile strength (more than a few pascals; see Methods). An albedo of 0.04 results in an object with dimensions of 800 m × 80 m × 80 m. The case of a contact or quasi-contact binary consisting of two elongated lobes can be rejected because it would require unrealistically high physical densities. Alternatively, if the object has no tensile strength, then the rotation axis must be the longest and its density could be in the range of that of asteroids. Because its rotation would be less stable is this case, we consider the cylindrical morphology to be more likely. For comparison,

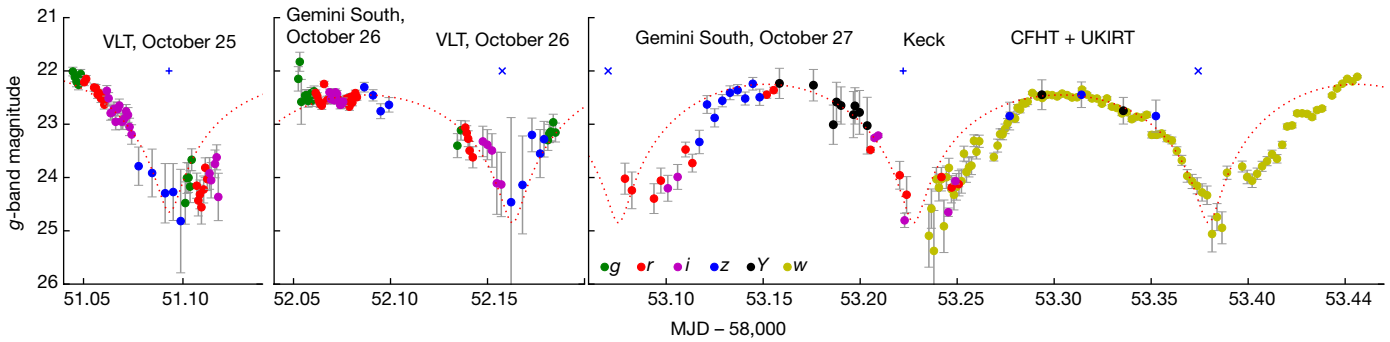

Figure 3 | Light curve of 'Oumuamua. All of the magnitudes have been scaled to the g-band magnitude using the measured colours, and to the geometry of October 25. Epochs are corrected for travel time for October 25. The error bars indicate 1σ photometric errors. The red dotted line corresponds to a 10:1:1 triaxial ellipsoid with a 20% variation in albedo across the surface, rotating with a 7.34 h period; the '+' and '×' symbols identify the two minima of the double-peaked light curve. MJD, modified Julian date.

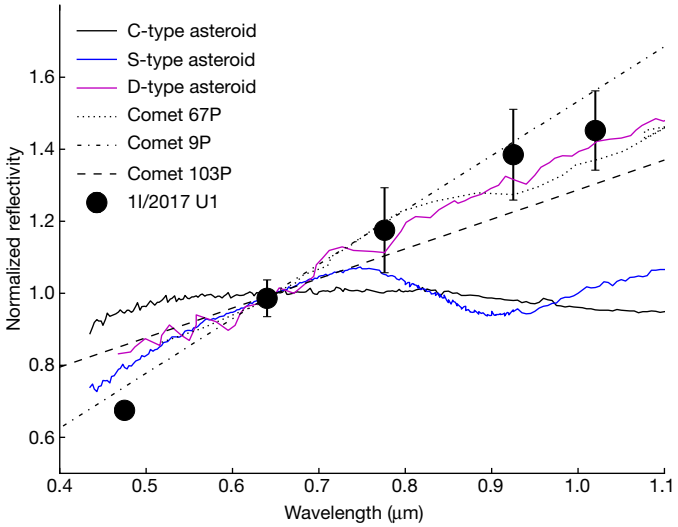

Figure 4 | Reflectivity of the surface of 'Oumuamua. The surface reflectivity of 'Oumuamua is consistent with D-type asteroids[10] and comets. Data are normalized to 1 at 0.65 μm and the error bars reflect the 1σ standard deviation.

ideal strengthless triaxial ellipsoids have a maximum light-curve amplitude of 0.9 mag (ref. 4). Nevertheless, five known objects[5] that are likely to have internal strength have maximum light-curve ranges of at least 2.2 mag, and the asteroid (1865) Cerberus (with a diameter of 1.6 km) has a 2.3 mag range[5].

Because a kilometre-scale object can exhibit such a large light-curve range, it may be expected that smaller objects such as 'Oumuamua are more likely to have greater mechanical strength and are thus capable of sustaining a highly elongated shape. However, there are few objects of comparable size in the Solar System that have light-curve ranges that approach that of 'Oumuamua, raising the question of why the first known ISO is so unusual.

It has been suggested[6] that there is a flux of very small (less than 100 μm) interstellar meteoroids from the debris disk around β Pictoris. So it is possible that 'Oumuamua originated from a nearby debris disk. The asymptotic radiant for 'Oumuamua is towards right ascension 18 h 42 min and declination +34.3° (±5′), near the current position of the Vega debris disk[7] at 18 h 36 min, +38.8°. However, the travel time to Earth from the distance of Vega is around 600,000 years, accounting for the proper motion of Vega. Therefore, 'Oumuamua is not likely to have been ejected from the Vega system. The outgoing asymptote is 23 h 52 min, +24.8°.

Alternatively, a close encounter between a long-period comet and a small undiscovered nearby planet[8] could possibly perturb the smaller object onto a hyperbolic orbit. For such a planet to remain undiscovered for so long, it must be located near the Galactic plane (which most near-Earth orbit (NEO) surveys avoid), whereas the radiant for 'Oumuamua has a Galactic latitude of around 16°. It is also possible that a more-distant, larger, undiscovered planet in the Solar System could have perturbed 'Oumuamua into an unbound orbit. The best estimate for the location of a distant planet of sufficient mass (approximately ten Earth masses) is many hundreds of astronomical units from the Sun[9], but an estimate of the orbital plane of such a planet does not contain the radiant for 'Oumuamua. Although we believe it unlikely that an undiscovered planet could have produced the motion of 'Oumuamua, we cannot yet rule it out. A deep search for distant planets in the radiant direction of 'Oumuamua would help to confirm or reject this possibility.

The heliocentric incoming velocity of 'Oumuamua in right-handed Galactic coordinates is $\boldsymbol{v}_\infty(U, V, W) = (-11.2, -22.4, -7.6)$ km s^{-1}. This velocity is remarkably close to the mean motion of stars in the solar neighbourhood[10], with an especially small deviation from the mean in U and W. Younger stars have smaller velocity dispersions than do older systems, so this close proximity to the exact local mean velocity suggests an origin in a young stellar system, although the possibility that 'Oumuamua has been orbiting the Galaxy for billions of years cannot be ruled out. This encounter has transformed the orbit of 'Oumuamua from one that is particularly close to the local mean to one that is typically dispersed from the mean, hinting that this encounter may be the first close approach to a star by 'Oumuamua and thus its first chance to lose volatiles.

The asteroidal nature of 'Oumuamua is surprising given that the predicted ratio of cometary to asteroidal material in the Oort cloud in the Solar System ranges from 200:1 to 10,000:1, depending on the chosen formation model for the Solar System[11]. We therefore expected that most ISOs would be cometary, assuming that the range of ratios in the Oort cloud was applicable to objects that were ejected into interstellar space. Asteroidal objects on long-period cometary orbits in the Solar System have only recently been discovered[11], and are known as Manx-type comets. A population of interstellar asteroids could have arisen from scattering events in their host system if major planets migrated through strong resonances and ejected objects with more mature, processed, inner-solar-system material than that of the objects in their Oort-cloud-equivalent. If typical ISOs are asteroid-like, then their number density could be much higher than contemporary limits[2,12]: current models assume that cometary material is more likely to be ejected and that comet-like ISOs should be the easiest to detect because of selection effects.

The discovery of 'Oumuamua suggests that there are probably additional ISOs in the Solar System at any given time and raises the prospect of many future ISO discoveries. These objects will enable elemental abundances in other solar systems to be measured and planetary formation theories to be tested. Calculating the formal influx number density of ISOs and predicting their future discovery rate by existing and planned sky surveys from the single 'Oumuamua discovery would require a detailed simulation of the ISO detection efficiency of the surveys[2], which is complicated by regular improvements to their operations. It is likely that the discovery of 'Oumuamua was made possible by recent improvements to the Pan-STARRS1 detection pipeline that resulted in an increased efficiency of finding trailed objects (previously some were rejected incorrectly as spurious detections). Our number density estimates suggest that there is always about one ISO of about 250 m diameter (assuming an albedo of 0.04) within one astronomical unit of the Sun, that is, interior to Earth's orbit (see Methods).

The discovery of an ISO adds a new component, albeit small, to the risk of an impact with Earth: an impact from an ISO would be far more energetic than one from a Solar System object with similar mass, owing to the larger impact speed. A meteorite that resulted from an impact with an ISO would have an age inconsistent with that of the Solar System, of which no example is yet known.

Online Content Methods, along with any additional Extended Data display items and Source Data, are available in the online version of the paper; references unique to these sections appear only in the online paper.

Received 1 November; accepted 10 November 2017.
Published online 20 November 2017.

1. Charnoz, S. & Morbidelli, A. Coupling dynamical and collisional evolution of small bodies: an application to the early ejection of planetesimals from the Jupiter–Saturn region. *Icarus* **166,** 141–156 (2003).
2. Engelhardt, T. *et al.* An observational upper limit on the interstellar number density of asteroids and comets. *Astron. J.* **153,** 133 (2017).
3. Williams, G. V. *MPEC 2017–U181: COMET C/2017 U1 (PANSTARRS)* http://www.minorplanetcenter.net/mpec/K17/K17UI1.html (2017).
4. Jeans, J. H. *Problems of Cosmogony and Stellar Dynamics* Ch. III, 35–43 (Cambridge Univ. Press, 1919).
5. Warner, B. D., Harris, A. W. & Pravec, P. The asteroid lightcurve database. *Icarus* **202,** 134–146 (2009).
6. Baggaley, W. J. Advanced meteor orbit radar observations of interstellar meteoroids. *J. Geophys. Res.* **105,** 10353–10361 (2000).
7. Holland, W. S. *et al.* Submillimetre images of dusty debris around nearby stars. *Nature* **392,** 788–791 (1998).

8. Volk, K. & Malhotra, R. The curiously warped mean plane of the Kuiper Belt. *Astron. J.* **154,** 62–77 (2017).
9. Batygin, K. & Brown, M. E. Evidence for a distant giant planet in the Solar System. *Astron. J.* **151,** 22–33 (2016).
10. Francis, C. & Anderson, E. Calculation of the local standard of rest from 20 574 local stars in the New Hipparcos Reduction with known radial velocities. *New Astron.* **14,** 615–629 (2009).
11. Meech, K. J. *et al.* Inner solar system material discovered in the Oort cloud. *Sci. Adv.* **2,** e1600038 (2016).
12. Francis, P. J. The demographics of long-period comets. *Astrophys. J.* **635,** 1348–1361 (2005).

Acknowledgements Pan-STARRS1 is supported by NASA under grant NNX14AM74G issued through the SSO Near Earth Object Observations Program. K.J.M., J.T.K. and J.V.K. acknowledge support through NSF awards AST1413736 and AST1617015. This work is based in part on observations collected at the European Organisation for Astronomical Research in the Southern Hemisphere under ESO programme 2100.C-5008(A), and in part on observations obtained under programme GS-2017B-DD-7 at the Gemini Observatory, which is operated by AURA under cooperative agreement with the NSF on behalf of the Gemini partnership: NSF (USA), NRC (Canada), CONICYT (Chile), MINCYT (Argentina) and MCT (Brazil). This work is based on observations obtained with MegaPrime/MegaCam, a joint project of CFHT and CEA/DAPNIA, at the Canada–France–Hawaii Telescope (CFHT), which is operated by the National Research Council (NRC) of Canada, the Institut National des Sciences de l'Univers of the Centre National de la Recherche Scientifique of France, and the University of Hawaii. The data presented herein were obtained at the W. M. Keck Observatory, which is operated as a scientific partnership between California Institute of Technology, the University of California and the National Aeronautics and Space Administration. This observatory was made possible by financial support from the W. M. Keck Foundation. UKIRT is owned by the University of Hawaii (UH) and operated by the UH Institute for Astronomy; operations are enabled through the cooperation of the East Asian Observatory. We thank all of the directors who evaluated the requests for telescope time and facilitated the execution of the programmes on the telescopes: L. Ferrarese (Gemini), R. Ivison (ESO), D. Simons (CFHT) and R. McLaren (UKIRT). We also thank the queue operators and support staff who made the data available. We thank K. Withington for processing the CFHT data, S. Isani for help with non-sidereal guiding, and W. Varricatt and M. Irwin for help with WFCAM non-sidereal scheduling. We thank K. Kimura (Director of the 'Imiloa Astronomy Center) and L. Kimura (a Hawaiian linguistics expert) for their suggestion of a name. We recognize and acknowledge the very significant cultural role and reverence that the summit of Maunakea has always had within the indigenous Hawaiian community. We are most fortunate to have the opportunity to conduct observations from this mountain.

Author Contributions K.J.M. led the team post-discovery, including securing the telescope time for characterization and preparing for observing, contributed to data reduction and performed the sublimation modelling. R.W. discovered 1I/2017 U1 in the Pan-STARRS data and, with M.M., realized that it had a hyperbolic orbit. J.T.K. performed all of the photometry, developed new pipeline software, and contributed to the shape interpretation and calculation of velocity relative to the local standard of rest. O.R.H. helped to secure the VLT time, prepared the VLT phase II programme, performed the initial data processing, and developed the rotational light-curve–colour solution and assessment of shape and its implications. R.J. calculated the spatial number density of ISOs. K.J.M., R.W., M.M., J.T.K., O.R.H. and R.J. contributed to the analysis of the data. M.M. performed all astrometry, contributed to observing preparation, integrated the orbit backwards to determine the asymptote and developed the optimum strategy for future astrometry. R.J.W. contributed to the discovery, obtained early CFHT observations that revealed the asteroidal nature, alerted K.J.M. to the need for mobilization and prepared the CFHT observing. K.C.C. contributed to the UKIRT photometry and the calculation of motion with respect to the local standard of rest. J.V.K. prepared the Gemini phase II programme and oversaw the observations. K.J.M., R.W., M.M., J.T.K., O.R.H., R.J., R.J.W., K.C.C., J.V.K. and L.D. contributed to writing the paper. A.P. helped with the CFHT mosaic reductions. T.B. helped with the Keck observations. E.M. led the team that developed the PS1 image processing system, contributed Keck telescope time, performed the observing and reduced the data. M.E.H. supports the daily downloads for moving objects. H.F., C.W. and M.E.H. support the image processing pipeline system that makes the Pan-STARRS data possible. E.S.-L. is part of the team that examines the daily data. S.C. writes and maintains software for extracting moving objects from the PS1 data.

Author Information Reprints and permissions information is available at www.nature.com/reprints. The authors declare no competing financial interests. Readers are welcome to comment on the online version of the paper. Publisher's note: Springer Nature remains neutral with regard to jurisdictional claims in published maps and institutional affiliations. Correspondence and requests for materials should be addressed to K.J.M. (meech@ifa.hawaii.edu).

Reviewer Information *Nature* thanks P. Chodas and A. Fitzsimmons for their contribution to the peer review of this work.

METHODS

Discovery and orbit determination. The October 19 detection of 'Oumuamua by the Pan-STARRS1 telescope[3] used four sidereally tracked w_{P1}-band images obtained in poor seeing conditions (with a stellar FWHM of 2.2″) during normal survey observations for NEOs[13]. Two additional w_{P1}-band pre-discovery images from 2017 October 18 were then identified in images with stellar FWHMs of 1.8″ and 2.4″. It was not possible to detect low-level cometary activity in these images owing to poor seeing and the object being trailed.

Elliptical and parabolic heliocentric orbits both gave atypically large fit residuals when additional astrometry beyond the original detections were included. Follow-up observations with the ESA Optical Ground Station also did not fit and were blocked by the Minor Planet Center (MPC) automated routines as suspected outliers. Our investigation revealed that this object could be explained using a hyperbolic orbit with a preliminary eccentricity of $e \approx 1.13$, the largest ever recorded (the next largest of $e = 1.057$ being for comet Bowell and due to a Jupiter encounter). 'Oumuamua was first classified as an Aten-type object (semi-major axis $a = 0.74$ AU, $e = 0.449$, inclination $i = 10°$) when it was posted to the NEO confirmation page (NEOCP). The Aten-type orbit induced a 5′ error in the predicted location of the object 24 h later, which increased to 34′ after 48 h. The object was later classified as a Halley-family comet when the MPC revised the orbit to $a = 50$ AU, $e = 0.997$, $i = 107°$ after including the Catalina Sky Survey observations on October 20, and the ephemeris error for our pre-discovery observations decreased from 34′ to 0.5′. The object's orbit was seen to be clearly hyperbolic after the arc was extended to October 22 by our CFHT observations. With additional CFHT astrometry on 2017 October 22 UT (Fig. 1b), the eccentricity was revised to $e = 1.188 \pm 0.016$. With a total of 131 observations (11 of which were rejected as outliers), the orbital eccentricity of 'Oumuamua is now hyperbolic at the $>100\sigma$ confidence level, having a barycentric eccentricity of $e = 1.1929 \pm 0.0006$ (Extended Data Table 1). The two most important planetary close approaches were with Earth (0.16 AU ≈ 16 Hill radii) and Jupiter (4.82 AU ≈ 14 Hill radii), but even they are too distant to perturb 'Oumuamua substantially during its approach towards the Sun (nevertheless, these perturbations have been modelled in the discussion presented here).

Improvements in survey strategy. Many objects that are first detected when moving as fast as 'Oumuamua are lost if they are not immediately targeted for more observations. The ISO discovery rate could be improved by increasing the survey depth, the sky coverage rate and search strategies. The surveys could also self-follow-up[14], but this would reduce the NEO discovery rate from which the surveys derive their funding. The ISO detection rate may also be improved with enhanced source detection algorithms for trailed and non-stellar sources in images. One reason for the inefficiency in detecting ISOs is a biased search strategy. ISOs with high rates of motion may have been posted to the NEOCP, but recovery efforts would have targeted incorrect positions, because these positions were predicted assuming that the objects are small, nearby and have elliptical orbits. In general, one night after discovery, an ISO would be located to the west of the predicted position of an NEO with similar motion, and outside the region that is assumed as a realistic uncertainty for regular elliptical orbits. For 'Oumuamua, the geometry was such that some elliptical solutions overlapped with the true hyperbolic solution and its predicted location on the sky was therefore serendipitously imaged in follow-up observations.

Further reducing the ISO discovery rate, two-thirds of ISOs that display cometary activity would not rank highly enough to be posted to the NEOCP upon discovery, because the ranking is based only on apparent rates of motion[2]. Instead, the detections would have to be identified as unusual (cometary) on the basis of their non-stellar point-spread function; subsequent targeted follow-up observations would then allow identification of ISOs.

Discovery and characterization observations. *Pan-STARRS1.* The Panoramic Survey Telescope and Rapid Response System[15] (Pan-STARRS1) is a 1.8-m-diameter wide-field astronomical imaging and data processing facility, with a 3° field of view with 0.25″ pixels. The data are processed to remove instrumental artefacts, and most objects are detected automatically and calibrated photometrically and astrometrically[14,16,17]. Fast-moving objects that leave trails on the image, such as 'Oumuamua, must be re-measured before submission to the MPC.

Canada–France–Hawaii Telescope (CFHT). Observations taken with the 3.6-m-diameter CFHT used the MegaCam wide-field imager, an array of forty $2,048 \times 4,612$ pixel CCDs with a plate scale of 0.187″ per pixel and a 1.1 deg^2 field of view. The data were obtained using queue service observing and processed to remove the instrumental signature through the Elixir pipeline[18]. Three 60-s exposures were obtained on 2017 October 22 UT using a wide *gri*-band filter with FWHM = 0.5″ seeing. The exposures were tracked at the predicted motion of the object and obtained in excellent conditions (Fig. 1b). The immediate area surrounding the object was searched for faint companions with similar motion but none was found. 'Oumuamua was at a heliocentric distance of 1.22 AU, just 43 days past perihelion (0.25 AU) on September 9. A series of MegaCam observations was also obtained on 2017 October 27 UT using the wide *gri*-band filter to obtain a light curve. Integration times were initially 70 s but were increased to 180 s to improve the signal-to-noise ratio. The weather during the period October 23–26 on Maunakea was poor and no observations could be obtained.

Gemini South Telescope. We were awarded 3.5 h of Director's Discretionary time for rapid observations of 'Oumuamua using the 8 m Gemini South Telescope. Data were obtained using the Gemini Multi-Object Spectrograph (GMOS) in imaging mode, which uses three $2,048 \times 4,176$ Hamamatsu chips. The data were obtained through Sloan Digital Sky Survey (SDSS) filters using queue service observing. The detector was read out with pixels binned 2×2 with slow read (read noise of 3.98 electrons) and low gain (1.83 electrons per analogue–digital unit (ADU)). Exposures were kept to 30 s to minimize trailing.

Very Large Telescope (VLT). Observations were performed at the ESO 8.2-m-diameter VLT UT1 on Paranal, Chile, using Director's Discretionary time, tracking the object with short exposures (30 s) to minimize trailing of the stars. We used the FORS2[19] instrument and the g-HIGH+115, R-SPECIAL+76, I-BESS+77 and z-Gunn+78 filters with the 'red' CCD, a $2,000 \times 4,000$ pixel MIT detector. The pixels were read-binned 2×2 resulting in an image scale of 0.25″ per pixel.

United Kingdom Infrared Telescope (UKIRT). The data were obtained using the 3.8-m-diameter UKIRT in 30-s frames while tracking non-sidereally according to the 'Oumuamua ephemeris. Alternating blocks in z and Y bands were de-trended, registered and stacked manually. The magnitudes are calibrated in the SDSS (z) and UKIDSS (Y) systems.

Keck 2 Telescope. Observations were performed on the Keck 2 10 m telescope using DEIMOS (DEep Imaging Multi-Object Spectrograph) in imaging mode. DEIMOS has a 2×4 array of $2,000 \times 4,000$ pixel MIT/Lincoln Labs CCDs to cover the full spectral range. In imaging mode, four of these detectors are illuminated by the sky with a plate scale of 0.1185″ per 15-μm pixel. The object was observed with CCD number 6 using non-sidereal guiding or tracking. Image quality during these observations was 1.5″ (FWHM). A total of 18 exposures were obtained of the object using Johnson B, R and I filters with 100-s exposures. Guiding failed during two of these exposures; in the remaining 16 exposures, the object was not detected in the two B-band images, or in five of the images near the light-curve minimum. Owing to substantial residual background variations in the images, photometry was measured for the object using a 1.8″-diameter aperture, corrected to the standard 4″ aperture using bright stars in a sidereal-tracked image in the same period. Zero-points and colour corrections were measured to transform the photometry to SDSS magnitudes in the r and i bands using stars from the PS1 3π survey[15,16], assuming a colour of $r - i = 0.3$ mag.

Visual-band CCD data reduction. We reduced all visual-band CCD data using custom code for bias subtraction and flat-fielding to establish a uniform detector response. We use the Terapix/Astromatic tools[20] to fit world coordinates (right ascension and declination) using reference stars from the SDSS and 2MASS catalogues. We used expanded SExtractor[20] automatic apertures to measure the magnitudes of trailed stars and computed a photometric zero-point for each image using stars from the PS1 database[16] 3π survey[15] or the SDSS[21]. The final *griz* magnitudes are in the SDSS system, and the Y magnitudes in the UKIDSS system. Finally, we measured the apparent magnitude of 'Oumuamua by summing the flux inside a 4″-diameter aperture placed at the adjusted ephemeris location and correcting for the zero-point.

Solving for the rotation period and colours. The light-curve data were first corrected for the observing geometry to normalize the heliocentric and geocentric distances to those of October 25.0, and preliminary colour corrections were applied to all of the data points. An initial rotation period was determined using the phase dispersion minimization (PDM) technique[22]. The colour indexes ($g - r$, $g - i$, $g - z$ and $g - Y$) were then included in the PDM to minimize the dispersion between the light-curve segments to obtain the final period and colours.

We estimated the uncertainty on the period and colours by 'scanning' through each value individually. The phased light curve for the values at the limit of the interval of confidence was also checked visually and determined to be "almost but not quite as good" as the best fit. Rotation periods were scanned in the range 2–20 h to ensure that no other period could reproduce the observations. In particular, the half-period of about 3.65 h fails to produce a satisfactory single-peaked phased curve (which would be difficult to explain physically). A period of 11.0 h is marginally acceptable with the PDM metric, but produces a triple-peaked light curve.

Shape and size. The light curve of a triaxial ellipsoid[23] with axis ratio $a > b > c$ was fitted to the light curve for 'Oumuamua. Because the geometry of the rotation axis is unknown, the aspect angle (between the line of sight and the rotation axis) was set to the most probable value of 90°, resulting in a lower limit on the elongation. Asteroids usually rotate on their shortest axis (c) for stability. The fit

yields an axis ratio of 10:1:c, with large uncertainties on $a = 10 \pm 1$ (which are dominated by the noise of the faintest points; see Fig. 3). The value of c is not constrained directly by the light curve. We accounted for a small asymmetry between the light-curve maxima, with a periodic signal of 0.2 mag amplitude intended to represent a relative albedo variation of 20% across the surface. Because the albedo and geometric cross-section are degenerate, this interpretation is not strong. The resulting model is not unique but is useful to guide the eye. It is clear that light curve for 'Oumuamua has systematic deviations with respect to the fitted ellipsoid and these probably correspond to large areas where the object is flat or concave (flat and concave cannot be distinguished by the light curve because they produce the same cross-section). A roughly spherical object would require extreme variations in albedo to reproduce the range and the sharp minima of the light curve, but on the basis of our current understanding of the surfaces of most asteroids in the Solar System and the absence of any sign of volatiles this is unlikely.

The brightest ($g = 22.15$ mag) and faintest ($g = 24.65$ mag) light-curve values differ by 2.5 mag, which implies a 10:1 axis ratio for two sides of the ellipsoid. The median g-band magnitude can be converted to an absolute magnitude of $H_V = 22.4$ mag (in the H–G asteroid photometric system[24]) after accounting for the colours of 'Oumuamua. Assuming a cometary albedo of 0.04 yields an effective radius of 102 ± 4 m (the uncertainties are based on only the uncertainties in magnitude). Kuiper-belt objects have a range of albedos (0.04–0.28), and higher albedos are associated with icy objects[25]. 'Oumuamua is not icy, and billions of years of irradiation by Galactic cosmic rays and ionizing radiation should darken its surface; we therefore assume that the surface has a low albedo. It is meaningless to convert the brightest and faintest magnitudes into linear dimensions directly, because a/c is not constrained directly by the light curve.

However, the c axis can be constrained together with the density of the object ρ and its albedo p, so that the πpac and πpbc cross-sections match the light-curve maximum and minimum, and the gravity at the tip of the a radius matches the centrifugal force. An additional constraint comes from the fact that the rotation must take place along the shortest axis, so $a > b > c$, or possibly along the longest axis, with $c > a > b$ (rotation along the intermediate axis is not stable). The densities that correspond to a strengthless short-axis rotator are unphysically high (more than 20,000 kg m^{-3}), suggesting that a long cylindrical short-axis rotator must have some internal tensile strength and ruling out a binary or close binary. To estimate this strength, we estimated the centrifugal force and gravitation force by cutting the object into two parts along its long axis. Scanning density values of 500–10,000 kg m^{-3} lead to a very moderate minimum required strength of 3 Pa. With $b = c$ and an albedo of $p = 0.2$, this strength results in radii of 180 m × 18 m × 18 m, or 400 m × 40 m × 40 m with $p = 0.04$.

Alternatively, a long-axis rotator can be held together by gravity for densities of more than 1,500 kg m^{-3}, resulting in physical radii of about $a \times b \times c = 40$ m × 4 m × 80 m for an asteroid-like albedo of $p = 0.2$ or 90 m × 9 m × 180 m for a dark albedo of $p = 0.04$. The density and c axis estimates are both lower limits.

Assessment of lack of activity. To reach the faintest possible surface brightness, a stack of the g- and r-band images from Gemini and VLT was produced, totalling 1,920 s of exposure time. By coincidence, the photometric zero-points of these two filters are virtually equal, with $ZPg = ZPr = 27.98$ (for ADU per second per pixel). The profile of the object was estimated by averaging its flux in annuli. A Moffat function[26] was adjusted to an average profile, resulting in a Moffat function parameter $\alpha = 1.1''$, which corresponds to a FWHM of 0.87″. The individual pixels and profiles are displayed in Fig. 1. The Moffat profile represents the profile of the object well out to about 2″, where the sky noise dominates. We assume that all of the flux difference between the profile of the object and the Moffat profile corresponds to a coma; this gives $g_{\mathrm{coma}} = 25.8$ mag for the ring between 1″ and 2″ (to be compared to $g_{\mathrm{'Oumuamua}} = 22.5$ mag). This magnitude can be converted into a total diffusing area of dust grains. Assuming an albedo of 0.04, a bulk density of 1,000 kg m^{-3} (typical for fluffy cometary grains seen from the Rosetta mission[27]) and a grain radius $a = 1\,\mu$m, up to 0.5 kg of dust could be present around the object; assuming an albedo of 0.2, a bulk density of 3,000 kg m^{-3} (typical compact cometary grains[27]) and a grain radius $a = 1\,\mu$m, up to 0.3 kg of dust could be present.

At larger radii from the object, any (not visible) coma would be fainter than the noise background (0.147 ± 0.005 ADU per second per pixel in 0.25″ pixels). The 3σ (5σ) brightness limits from dust correspond to surface brightnesses of $g = r = 30.4(29.8) \pm 0.05$ mag arcsec^{-2}. Using the same assumptions as above, up to 13 g (8 g) per pixel of cometary dust could be present at the 3σ (5σ) level, and up to 8 g (4 g) of asteroidal dust. In the 2″–2.5″ annulus (which covers around 100 pixels), this dust mass could represent up to 1 kg.

Most long-period comets (LPCs) were originally scattered into the Oort cloud during the formation of the Solar System. The comets that we see now are being dislodged from the Oort cloud and returned to the Solar System after around 4.6 Gyr of exposure to an interstellar environment, yet most are active objects and are expected to be active for thousands of perihelion passages. Given that LPCs retain their volatiles over timescales of billions of years and the fact that 'Oumuamua has been at the temperatures of interstellar space for a long time, any ice should have survived for billions of years. However, because no similarly sized inactive objects on LPC orbits have been discovered in the Solar System, and Manx-type comets are rare, it is difficult to reconcile the lack of volatiles on 'Oumuamua with our current understanding of LPC formation and composition. A water-ice thermal sublimation model[28] shows that the maximum dust production for 1-μm grains that can be sustained and remain below the coma detection limits mentioned above is 1.668 10^{-3} kg s^{-1} (assuming a dust-to-gas ratio of 1). This production rate corresponds to a few kilograms within the aperture and is in agreement with the estimate obtained by comparing the surface brightness profile of 'Oumuamua to the Moffat stellar profile.

Estimating the ISO number density. We estimate the ISO number density (ρ_{IS})—that is, the spatial number density of ISOs far from the influence of any stars—by scaling from a previous 90% upper confidence limit[2] on ρ_{IS} of 2.4×10^{-2} au^{-3} for inactive (asteroidal) objects with $H < 19$, assuming an albedo of 0.04, typical of cometary nuclei (corresponding roughly to objects with diameters or more than 0.5 km). This limit is based on the lack of discovery of any ISOs during around 18 integrated years of surveying using the Pan-STARRS1[15] and Catalina Sky[29] surveys. These surveys subsequently acquired another approximately 12 years of data, so we normalize the survey time on the basis of the discovery rate of $H < 22$ NEOs (http://www.minorplanetcenter.net/iau/lists/YearlyBreakdown.html) during and subsequent to the original time period. Owing to surveying, hardware and software improvements, the surveys have since discovered roughly 1,930 $H < 22$ NEOs compared to about 1,740 objects during the original study. We extrapolate from the $H < 19$ (>0.5 km diameter) size to $H < 22$ using the size–frequency distribution for a self-similar collisional cascade[30] of $N(<H) \propto 10^{0.5H}$ because this distribution is broadly representative of most small-body populations in the Solar System in this size range[31]. Finally, we account for the decreased survey depth (geocentric distance) for objects with $H = 19$ mag and $H = 22$ mag: the Pan-STARRS1 system with a V-band limiting magnitude[14] of about 21.7 mag can detect objects of these absolute magnitudes out to geocentric distances of only about 1.4 au and 0.55 au, respectively. Assuming that most ISOs are inactive, asteroid-like objects similar to 'Oumuamua, the interstellar ISO number density of $\rho_{\mathrm{IS}}(H < 19) \approx 0.003$ au^{-3} is close to previous upper confidence limits[2]. Scaling down in size to $H = 22$ mag, comparable to 'Oumuamua, and accounting for the density enhancement by a factor of three due to the Sun's gravity[2], we estimate that there is always about one $H < 22$ mag ISO (about 250 m diameter assuming a visual albedo $p = 0.04$) within 1 au of Sun, that is, interior to Earth's orbit.

Code availability. The software used to perform DEIMOS photometry is available from http://svn.pan-starrs.ifa.hawaii.edu/trac/ipp/browser. The UKIRT data were detrended using the standard WFCAM data processing pipeline. We have opted not to make the custom calibration and photometry software used to reduce imaging data from the VLT, Gemini and CFHT available because the components relevant to this work cannot be readily isolated. Various short, custom scripts were developed for the analysis; they are available on request. We have also opted not to make the sublimation model software available because it is being upgraded.

Data availability. The GMOS and ESO FORS2 raw data will be available in the Gemini and ESO archives, respectively, after the expiration of the proprietary period. CFHT raw and reduced images are available on request. The raw UKIRT data will become available from the UKIRT archive; reduced data are available on request. DEIMOS raw images are available on request.

13. Wainscoat, R. J. *et al.* The Pan-STARRS search for near Earth objects. *IAU Symp.* **318,** 293–298 (2016).
14. Denneau, L. *et al.* The Pan-STARRS moving object processing system. *Publ. Astron. Soc. Pacif.* **125,** 357–395 (2013).
15. Chambers, K. C. *et al.* The Pan-STARRS1 Surveys. Preprint at https://arxiv.org/abs/1612.05560 (2016).
16. Magnier, E. A. *et al.* Pan-STARRS photometric and astrometric calibration. Preprint at https://arxiv.org/abs/1612.05242 (2016).
17. Magnier, E. A. *et al.* Pan-STARRS pixel analysis: source detection and characterization. Preprint at https://arxiv.org/abs/1612.05244 (2016).
18. Magnier, E. A. & Cuillandre, J.-C. The Elixir system: data characterization and calibration at the Canada-France-Hawaii telescope. *Publ. Astron. Soc. Pacif.* **116,** 449–464 (2004).
19. Appenzeller, I. *et al.* Successful commissioning of FORS1 — the first optical instrument on the VLT. *Messenger (Los Angel.)* **94,** 1–6 (1998).
20. Bertin, E. & Arnouts, S. SExtractor: software for source extraction. *Astron. Astrophys. Suppl. Ser.* **117,** 393–404 (1996).
21. Fukugita, M. *et al.* The Sloan Digital Sky Survey photometric system. *Astron. J.* **111,** 1748–1756 (1996).
22. Stellingwerf, R. F. Period determination using phase dispersion minimization. *Astrophys. J.* **224,** 953–960 (1978).

23. Detal, A. *et al.* Pole, albedo and shape of the minor planets 624 Hektor and 43 Ariadne: two tests for comparing four different pole determination methods. *Astron. Astrophys.* **281,** 269–280 (1994).
24. Bowell, E. *et al.* in *Asteroids II* (eds Binzel, R. *et al.*) 549–556 (Univ. Arizona Press, 1989).
25. Mommert, M. *et al.* TNOs are cool: a survey of the trans-Neptunian region. V. Physical characterization of 18 Plutinos using Herschel-PACS observations. *Astron. Astrophys.* **541,** A93 (2012).
26. Trujillo, I., Aguerri, J. A. L., Cepa, J. & Gutiérrez, C. M. The effects of seeing on Sérsic profiles – II. The Moffat PSF. *Mon. Not. R. Astron. Soc.* **328,** 977–985 (2001).
27. Fulle, M., and 40 colleagues. Density and charge of pristine fluffy particles from comet 67P/Churyumov–Gerasimenko. *Astrophys. J.* **802,** L12 (2015).
28. Meech, K. J., Jewitt, D. & Ricker, G. R. Early photometry of comet p/Halley — development of the coma. *Icarus* **66,** 561–574 (1986).
29. Christensen, E. *et al.* The Catalina Sky Survey: current and future work. In *AAS/DPS Meeting Abstracts* Vol. 44, 210.13 (AAS, 2012).
30. Dohnanyi, J. S. Collisional model of asteroids and their debris. *J. Geophys. Res.* **74,** 2531–2554 (1969).
31. Jedicke, R., Larsen, J. & Spahr, T. in *Asteroids III* (eds Bottke, W. F. Jr *et al.*) 71–87 (Univ. Arizona Press, 2002).

Extended Data Table 1 | Orbital elements of 'Oumuamua determined from observations on 2017 October 14–30

Element	Heliocentric	Barycentric†
v_∞ (km/s)	-	26.15 ± 0.05
q (au)	0.25383 ± 0.00023	0.25066 ± 0.00023
e	1.1956 ± 0.0006	1.1929 ± 0.0006
i (deg)	122.545 ± 0.021	122.592 ± 0.021
Ω (deg)	24.6056 ± 0.0009	24.2570 ± 0.0009
ω (deg)	241.43 ± 0.04	241.44 ± 0.04
T	2017-09-09.461 ± 0.004	2017-09-09.091 ± 0.004
Epoch	2017-09-09.0	1838-01-01.0

The elements were integrated backwards in time until 'Oumuamua was 1,000 AU from the Sun to remove any possible effects from close encounters during the incoming trajectory. The time-of-passage at pericentre (T) should be interpreted as the peribarion in this case. The elements were computed using the software *Find_Orb* by Bill Gray.
†The barycentric elements account for periodic terms connected with the motion of the Sun around the barycentre.